Brillouin-scattering study of the elastic anomalies at the structural phase transition in anthracene-tetracyanobenzene

C. Ecolivet
Groupe de Physique Cristalline, Campus de Beaulieu, 35042 Rennes CEDEX, France

A. Mierzejewski
Institute of Organic and Physical Chemistry, Technical University of Wroclaw, 50-370 Wroclaw, Poland
(Received 2 April 1990)

Brillouin-scattering experiments performed at room temperature indicate unambiguous relations between the crystalline structure and the optical and elastic properties of this charge-transfer crystal. The largest refractive index and the large longitudinal sound velocity are found along the molecular long axis direction, which is $[20\bar{1}]$. All the elastic constants are determined, and the anisotropy of the derived linear compressibility is found in reasonably good agreement with the thermal-expansion anisotropy. Two kinds of elastic anomalies have been recorded at low temperatures and analyzed as being mainly due to an interaction that occurs along the $[20\bar{1}]$ direction. Elastic anomalies of relaxational character as large as 22% have been recorded, and a strong temperature dispersion allows the determination, in the low-temperature phase, of the order-parameter relaxation time $5\times10^{-11}(T_c-T)^{-1}$ s K^{-1}.

INTRODUCTION

Anthracene-tetracyanobenzene (A-TCNB) is a weak charge-transfer (CT) complex that exhibits at about 210 K a structural phase transition (SPT) that presents typical features of both displacive and order-disorder regimes. Earlier resonance experiments,[1-5] which often used triplet exciton dynamics as a probe of molecular environment, yielded to a weakly first-order structural phase transition that exhibits a typical order-disorder behavior. This behavior was also confirmed by the first Raman experiment,[6] which did not detect any soft mode in the low-frequency region. A molecular model based on a four-site picture was elaborated,[4] which reasonably agrees with exciton dynamics. However, another model[3] gave a continuous variation of the anthracene orientation that could also have been interpreted as a displacive behavior. It is only recently that an exhaustive Raman study on high-optical-quality-oriented single crystals[7] revealed the existence of a soft optical mode, which, however, presents the unusual feature that the frequency of its maximum seems to vanish below the transition temperature.

X-ray studies of this crystal showed that this (SPT) is nonferroic; i.e., the high- and low-temperature structures belong to the monoclinic symmetry. The high-temperature spatial group is $C2/m$ with one complex in the primitive cell,[8] whereas the symmetry is slightly lowered in the $P2_1/a$ group of the low-temperature phase.[9] In this structure, the two complex molecules of the unit cell are now only related by a glide plane or a twofold helicoïdal axis. More recent crystallographic studies also reflect the same duality in the displacive order-disorder description of this SPT. Boeyens and Levendis[10] have interpreted their anisotropic thermal libration data as a static disorder, whereas Lefebvre *et al.*[11] treated similar data and obtained a single broad peak in the orientational probability function, which clearly indicates a displacive mechanism for this SPT. With this same treatment, a double peak was found by the same authors in naphthalene-TCNB showing unambiguously an order-disorder regime for this other CT crystal.

Let us now have a look at the packing of A-TCNB; since this crystal is a weak CT crystal, it is built of mixed stacks of quasiparallel donor (A) and acceptor (TCNB) molecules. The stack axis is **c**, but the normals to the molecular planes are inclined at about 20° for TCNB and 22° for anthracene. This inclination and the size of the molecules cause the crystal to be composed of layers consisting of (102) planes, where A and TCNB molecules align their long axes along the $[20\bar{1}]$ direction in the high-temperature phase. Actually, in that phase, A molecules are orientationally disordered with respect to a libration movement with its axis perpendicular to the molecular plane. This disorder mainly results from steric hindrance due to the next in-plane TCNB neighbor, the distance of which between its nitrogen atom and the hydrogen atom of the A molecule equals exactly the sum of the Van der Waals radii (2.60 Å).[11] In the low-temperature phase, A molecules rotate to produce antiferro-orientational modulation, the rotation angle being about ±8° at 65 K.

Recently, theoretical papers have first suggested the existence of a soft mode,[12] then harmonic lattice-dynamic calculations[13] have described with a reasonable agreement the vibrational frequencies observed by Raman scattering in both phases. However, such harmonic models fail to describe the complex soft-mode behavior, and a new theoretical model has been proposed,[14] which is

based on the coupling difference between the interactions in the (**a**,**b**) planes and along the **c** direction. In case of a large anisotropy, simulation studies[15] suggest the occurrence of a nonclassical soft-mode evolution. Such an anisotropy would, for example, take into consideration that interactions in the layers would lead to a displacive transition, whereas interactions between layers would be so small that they would lead to an order-disorder regime. These interactions could generate instabilities at different temperatures; this is the reason that the large dispersion in the reported transition temperatures between 196 and 215 K was intriguing. It might have been that the different techniques were probing different phenomena with different responses, or a more probable explanation could be a large sensitivity of T_c to impurities or defects. In order to avoid such a drawback we managed to perform different experiments on the same crystal or on parts on the same crystal. A preliminary report[16] does not indicate any significant difference between the transition temperatures detected by differential scanning calorimetry (DSC), Brillouin scattering, Raman scattering, and also by NMR and neutron scattering.

We report here about the elastic properties of *A*-TCNB and how they relate to its structure and its components. We also give detailed experimental results concerning the elastic anomalies that occur at this phase transition. Usually sound-velocity anomalies are quite visible, and since they are produced by the coupling of ordering quantities with strain, they can give valuable results for the understanding of the transition.

EXPERIMENTS AND ROOM-TEMPERATURE RESULTS

The Brillouin scattering setup, which uses a five-pass computer controlled Fabry Perot interferometer, has already been extensively described,[17] but due to the red-orange color of this crystal, we used the 6471-Å line of a krypton ion laser with a limited power of 80 mW in order to avoid the heating of the scattering volume. We have actually checked the onset of absorption at room temperature, and we have found two different wavelengths depending on the polarization: 5550 Å for polarization along **b** and 5750 Å along **a**: both wavelengths are far enough from the laser wavelength and avoid heating.

A large crystal of good optical quality was grown according to the method described in Ref. 7, then cleaved into two parts along a (010) plane. One of these halves cut along **a**, **b**, and **c*** was used in our experiments, the other one being used for NMR, DSC, and Raman scattering studies.

Low-temperature experiments were performed inside a Meric cryostat, where the temperature of the sample is controlled by a temperature-regulated nitrogen-gas flow. This ensures a minimal thermal gradient all over the sample as well as a temperature stability better than 0.1 K by using a three-term regulation.

The refractive indices have been measured at 6471 Å at room temperature by using the following procedure. First n_{c^*}, was measured by a prism method; $n_{c^*}=1.68$, then Brillouin backscattering was performed along the **a** and **c*** directions, which, according to the Brillouin shift formula,

$$\nu_B=\pm\frac{V}{\lambda_0}(n_i^2+n_s^2-2n_in_s\cos\theta)^{1/2}\ , \tag{1}$$

allows the determination of, respectively, n_b/n_{c^*} and n_a/n_b by rotating the beam polarization. In the above equation, n_i and n_s are the refractive indices for the incident and scattered beams, λ_0 is the laser wavelength, and V is the phase velocity of the acoustic wave selected by the scattering angle θ, which here equals 180°.

The ratio of the principal refractive indices $\beta=n_\gamma/n_\alpha$ is obtained from Brillouin backscattering along **b**. Using crystal optics relations in the frame defined by principal refractive indices directions, we can write

$$\frac{1}{n_\varphi^2}=\frac{\sin^2\varphi}{n_\alpha^2}+\frac{\cos^2\varphi}{n_\gamma^2}\ , \tag{2}$$

where n_φ is the refractive index for a ray polarized in the (**a**,**c**) plane and propagating within this plane at an angle φ of the direction corresponding to n_γ. Due to the monoclinic symmetry, the direction of n_γ is different from **a**, but the angle φ_1 between **a** and the principal direction can be derived from Eq. (2) when applied to n_a and n_{c^*}, which consequently determines the values of n_γ and n_α:

$$\cos^2\varphi_1=\frac{1-\beta^2b^2}{(1-\beta^2)(1+b^2)} \tag{3}$$

with $b=n_a/n_{c^*}$. This gives here, for $\beta=1.308$ and $b=1.205$, $\varphi_1\simeq\pm22°$; since the angle between the molecular long axes and the **a** direction is also about $-22°$, this indicates that the largest polarizability is actually along the molecular long axes, and consequently the plus sign of φ_1 can be discarded. The principal refractive indices values are, at 6471 Å,

$$n_\alpha=1.63,\ n_b=1.75,\ n_\gamma=2.13$$

with uncertainties in the percent range.

This birefringence is large but comparable to the one of anthracene crystals for which values of $(n_\gamma-n_\alpha)$ reported in the literature[18] are given between 0.40 and 0.65 at 5640 Å. However, the birefringence we have measured for pure TCNB is much smaller, 0.2, whereas refractive indices are of comparable magnitude:

$$n_\alpha=1.68,\ n_b=1.59,\ n_\gamma=1.78\ .$$

However, it is also plausible that in *A*-TCNB, n_γ be slightly increased by the proximity of the absorption band near 5750 Å, whereas pure TCNB and anthracene are completely transparent in the visible region.

The same kind of relation with the structure is also found in the anisotropy of the elastic properties. Through the use of a small-angle scattering geometry where the crystal is at 45° from the incident and scattered beams, we have measured the quasilongitudinal (QL) and quasitransverse (QT) sound velocities in the (**a**,**c**) plane, where the angular variation of these quantities is not

determined by symmetry. Figure 1 shows a projection of the structure and the velocity diagram in the (**a**,**c**) plane, where first a strong anisotropy of the QL velocity can be noticed with a ratio close to 1.5 for the extremum values, and second the direction of the maximum is found between $-20°$ and $-25°$ from the **a** axis. As in pure Van der Waals crystals,[19] this maximum corresponds to the molecular long axis, which, for a wave traveling along this direction, involves a larger number of intramolecular interactions than along any other direction. We can also compare the QL velocity values in the direction of the long molecular axis in pure anthracene and *A*-TCNB crystals, the larger one being recorded for *A*-TCNB with a value (4400 m/s) significantly larger than in pure anthracene (3900 m/s).[20] This difference unambiguously underlines the difference in packing between both structures.

In the following we will refer to two kinds of directions: The first will be true crystallographic directions and noted as [100]; the others will correspond to bisectors of crystalline directions, which are easily probed by right-angle scattering. They will be noted for convenience as ⟨101⟩. In that case, it does not refer to the crystallographic direction [101] but to the first bisector of the (**a**,**c***) plane.

Although the structure of pure TCNB is quite different,[11] the comparison of QL sound velocities between *A*-TCNB and pure TCNB is also interesting, so we measured the Brillouin shifts along some directions. The largest velocities are found along the [100] and ⟨011⟩ directions, respectively, 3500 m/s and 3580 m/s, whereas smaller velocities are observed along **b** (2750 m/s) and **c** (2940 m/s). This last value is also the smallest QL velocity observed in the (**a**,**c**) plane of *A*-TCNB and in pure anthracene; in both crystals it corresponds to the sound propagation in a direction perpendicular to the molecular planes.

In *A*-TCNB other acoustic mode velocities were also measured giving a total number of 98 different velocities. Among them, it is interesting to notice the very low velocity of the true transverse mode propagating along **c** ($\sim$500 m/s). Figure 2 represents the sound velocity diagrams in the (**b**,**c**) plane and a projection of the structure in that plane.

A least-mean-squares procedure was used to reduce velocity data to a set of 13 elastic constants that are related by the Christoffel equation:

$$\det|C_{ijkl}q_jq_l-\rho V^2\delta_{ik}|=0\ .$$

In the Voigt notation, this set is given in Table I. The smallest elastic constant is C_{44}, which is directly related to the above-mentioned transverse mode. It should be also noted that in a lattice-dynamics computation[13] this mode was found to be unstable as was another transverse mode related to C_{66}. In fact, neither of these modes has a zero velocity even if C_{44} is very small.

It is also interesting to consider the (**b**,**c***) velocity dia-

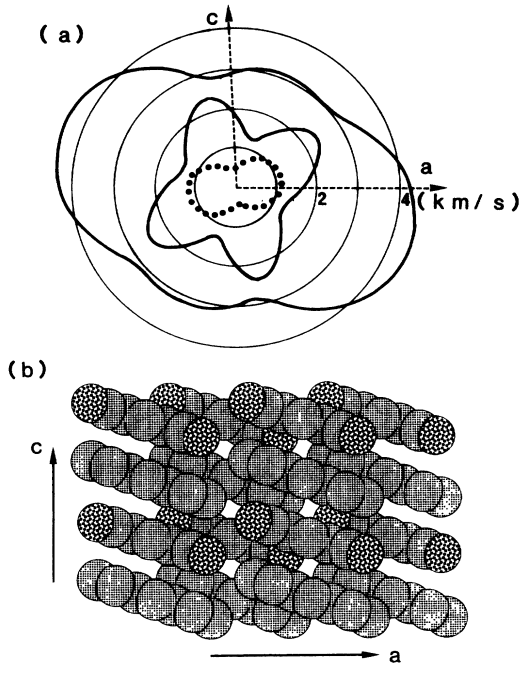

FIG. 1. Sound-velocity diagram (a) and projection of the molecular packing in the (**a**,**c**) plane (b). The dotted line corresponds to the true transverse mode polarized along **b**, whereas the two other lines are QT and QL modes. In the molecular projection, anthracene molecules are represented without hydrogen atoms. Carbon atoms are uniformally shaded, whereas nitrogen atoms are dotted.

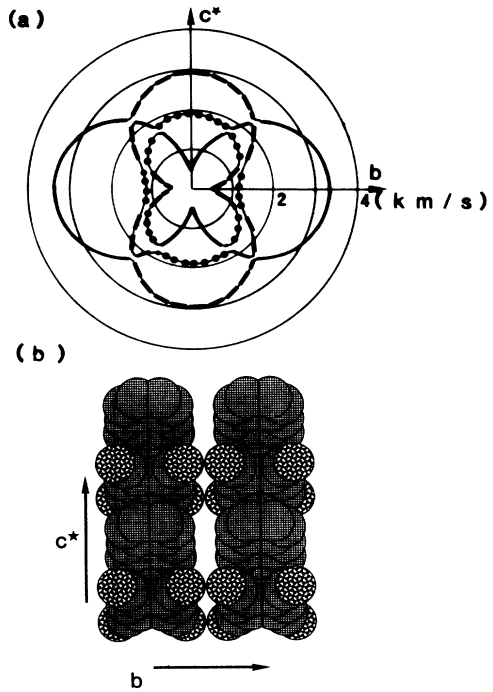

FIG. 2. Sound velocity (a) and projection of the molecular packing in the (**b**,**c***) plane (b). The three velocities never cross but dots are related to a QT mode mostly polarized along **a**, whereas dashes indicate a polarization along **c*** and the bold line indicates a polarization along **b**.

TABLE I. Elastic stiffness and compliance tensor components at room temperature.

ij	$C_{ij}\pm\Delta C_{ij}$ (GPa)		$S_{ij}\pm\Delta S_{ij}$ (10^{-12} m^2 N^{-1})	
11	22.40	0.41	84.1	3.8
22	14.67	0.53	80.8	6.2
33	10.91	0.27	125.6	8.1
44	0.31	0.03	3635	217
55	4.80	0.13	315.2	17.2
66	1.59	0.08	715.5	10
12	6.29	0.63	−30.1	−2.3
23	−0.64	−2.16	20.3	16.2
13	5.10	0.37	−51.2	−5.7
15	−4.84	−0.21	89.5	5.1
25	−1.34	−0.67	−13.0	5.4
35	1.23	0.15	−78.2	−1.1
46	0.25	0.05	−562.3	−53

gram. We notice that it could be easily broken down into three almost independent diagrams: one quasielliptic for transverse out-of-plane motions and two pairs of lobes for in-plane polarizations. These pairs of lobes have perpendicular axes, and the polarization of each mode belonging to one pair is directed along the axis of this pair of lobes, each lobe going nearly to zero for directions perpendicular to the lobe pair axis. These lobes can be approximately described by very simple equations such as $V'(\mathbf{q})=V(b)\mathbf{q}\cdot\mathbf{b}$ and $V''(\mathbf{q})=V(c^*)\mathbf{q}\cdot\mathbf{c}^*$. Such variations indicate that, in that plane, the elastic interactions are almost completely of compressive nature and the angular variations of the velocity of elastic waves polarized along **b** and **c*** are practically uncoupled, but since the (**b**,**c***) plane is not a symmetry plane, the related modes never cross in the diagram. The shape of this diagram can easily be related to the Christoffel equation, since for the (**b**,**c***) plane off-diagonal terms in the determinant are very small so that, in a fist-order approximation, the sound velocities in that plane can be written as

$$\begin{aligned}&\rho V_T^2\simeq\Gamma_{11}=C_{66}n_y^2+C_{55}n_z^2\ ,\\&\rho(V')^2\simeq\Gamma_{22}=C_{22}n_y^2+C_{44}n_z^2\simeq C_{22}n_y^2\ ,\\&\rho(V'')^2\simeq\Gamma_{33}=C_{33}n_z^2+C_{44}n_y^2\simeq C_{33}n_z^2\ .\end{aligned}\tag{4}$$

The projection of the crystal packing in the (**b**,**c***) plane in Fig. 2 reveals this weak transverse interaction, since it also reveals a columnar architecture with no diagonal links. The very small value of C_{44} describes an easy shearing of the stacks obtained by a lateral gliding motion of the molecular planes. This analysis agrees with models that assume weak orientational coupling along the stack axis. In the (**a**,**b**) plane the sound velocity diagram only displays a weak coupling between the QT modes (Fig. 3).

Another way of checking the consistency between the structure and the elastic properties is the comparison between the anisotropies of the thermal expansion and the linear compressibility tensors. Although these quantities are coming from derivatives of different orders of the

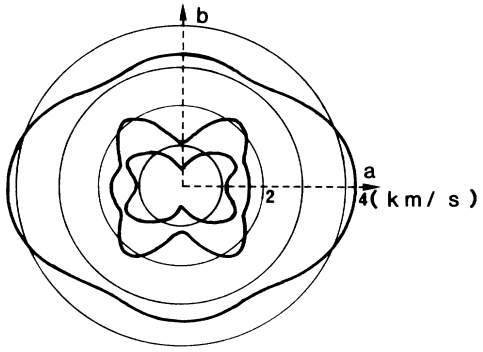

FIG. 3. Sound-velocity diagram in the (**a**,**b**) plane.

crystalline potential, their anisotropies are similar and, for instance, it is easily understandable that the linear compressibility is smaller, in a Van der Waals crystal, along the molecular long axis, whereas it is maximum perpendicular to parallel molecular planes; this behavior is also observed for the linear thermal expansion.

The thermal expansion tensor was measured by Lefebvre *et al.*[11] using x-ray diffraction. Along a direction **n** defined by its cosines n_1, n_2, n_3 the thermal expansion is given by

$$\alpha_{(\mathbf{n})}=\alpha_1 n_1^2+\alpha_2 n_2^2+\alpha_3 n_3^2+\alpha_5 n_1 n_3\tag{5}$$

in the frame defined by (**a**,**b**,**c***). For the linear compressibility, in the same frame, one obtains

$$\beta_{(\mathbf{n})}=A_1 n_1^2+A_2 n_2^2+A_3 n_3^2+A_5 n_1 n_3\ ,\tag{6}$$

where $A_i=\sum_{j=1}^{3}s_{ij}$, S_{ij} being the components of the elastic compliance tensor that are also given in Table I. Errors in S_{ij} were determined from the relation

$$\overleftrightarrow{\delta S}=-\overleftrightarrow{S}\,\overleftrightarrow{\delta C}\,\overleftrightarrow{S}\ .\tag{7}$$

It may be noticed that large relative errors are found for S_{23} and S_{25}, which are important terms in A_2, A_3, and A_5. Consequently, the comparison of α and β anisotropy is not so obvious. Nevertheless, the agreement between the ratios of the principal values is quite good: 120:50:14 for α and 104±24: 71±25: -4±16 for β. However, we do not, get a better agreement by giving a systematic sign to some ΔS_{ij} as might be thought by taking $\Delta\beta_1$ and $\Delta\beta_3$ positive and $\Delta\beta_2$ negative. Table II gives the nonzero components of the α and β tensors, and it can also be seen that a larger difference exists for the only nondiagonal component. This means that linear thermal

TABLE II. Components of the linear compressibility and thermal expansion tensors (Ref. 11) in the (**a**,**b**,**c***) frame.

A values (10^{-12} m^{2}n^{-1})	d values (10^{-6} K^{-1})
$A_1=2.8\pm11.8$	$\alpha_1=34$
$A_2=71\pm25$	$\alpha_2=50$
$A_3=94.7\pm30$	$\alpha_3=102$
$A_5=-2\pm11$	$\alpha_5=68$

expansion is the largest at 20° from the **c** axis, i.e., in the direction perpendicular to the molecular planes of the stacks, whereas the linear compressibility is found at its maximum value between ±10° from the **c** axis. This difference is probably not significant, and it seems that all these discrepancies find their origin in the poor determination of C_{23} and C_{25}. In conclusion to this room-temperature study, we can say that the charge-transfer character of this crystal does not significantly modify the elastic and thermal expansion anisotropies, which look exactly alike in pure Van der Waals crystals,[19] i.e., the sound-velocity anisotropy is directly determined by the anisotropy of the molecules and their packing, which for flat long molecules yields a maximum compressibility and thermal expansion perpendicular to the molecular planes.

LOW-TEMPERATURE EXPERIMENTS

We have measured the evolution with temperature of the velocity of 17 acoustic modes, and two different kinds of anomalies were recorded on different modes at low temperatures. The anomaly about which we report here first is the clearest one with respect to the critical-temperature determination, since a change of slope occurs at this temperature: 212 K. This angular point is mostly visible on true transverse modes propagating in the (**a**,**c**) plane. The direction where we have seen it most distinctly is $\langle 10\bar{1} \rangle$ (Fig. 4). This transverse mode is slow ($\sim$700 m/s) at room temperature and has a scattering efficiency comparable to that of the QL mode along this direction. No variation of the linewidth of this mode was detected in relation with this anomaly. The same anomaly is also detectable along **b** and **a** as shown in Fig. 5, which displays the variation of the phase velocity of all the elastic waves measured by Brillouin scattering between 180 and 235 K.

The second kind of anomaly is the one that is always, or at least very often, observed in structural phase transitions. It is detected through a negative jump of sound velocities near T_c when temperature is decreasing. In Brillouin scattering it results in a decrease of the Brillouin shift accompanied by a linewidth broadening that often occurs below T_c. We report below, the different modes affected by this anomaly in relation to their polarization, which was computed from the room-temperature elastic constants. The use of these constants is justified by a small difference of most of the sound velocities between 293 K and $T_c = 212$ K.

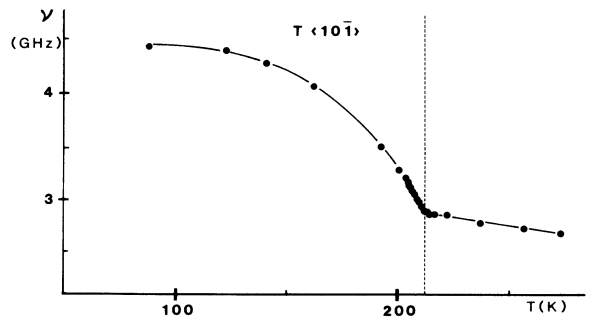

FIG. 4. Brillouin shift vs temperature of the true transverse mode propagating along $\langle 10\bar{1} \rangle$ between room temperature and 80 K (the line is a guide for the eye).

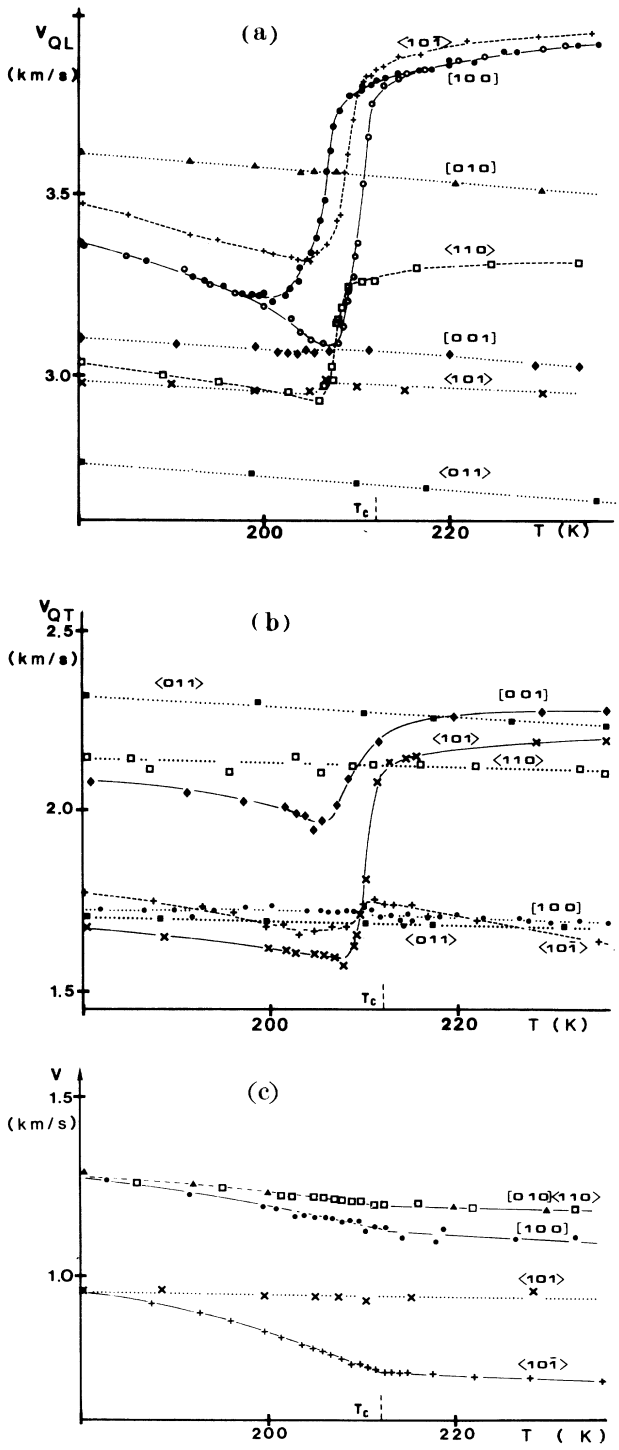

FIG. 5. Sound velocities vs temperature of all the measured modes plotted between 180 K and 235 K and computed from room-temperature refractive indices. ● and ○: (100), respectively in backscattering and small-angle scattering, +: $\langle 10\bar{1} \rangle$, ×: ⟨101⟩, ♦: (001), ■: ⟨011⟩, ▲: (010), and □: ⟨110⟩.

The largest relative anomalies are detected for modes polarized along the molecular long axis [20$\bar{1}$]. This is the case of the QL mode propagating along **a** and the QT mode propagating along the first bisector of the (**a**,**c***) plane, called here ⟨101⟩. They are, respectively, polarized at $-14°$ and $-24°$ from **a**. The magnitude of these anomalies which are quantified by $\Delta V^2/V^2(T_c)$, where $\Delta V^2 = V^2(T_c) - V^2_{\min}$ is larger than 30%, whereas it is in the 20% range for the QL modes propagating along the second bisector of (**a**,**c***) and of (**a**,**b**) , i.e., ⟨10$\bar{1}$⟩ and ⟨110⟩. Comparable but still smaller relative anomalies are observed for the QT modes propagating along **c*** and ⟨10$\bar{1}$⟩, whereas barely detectable anomalies occur for the QL mode along ⟨101⟩ and [001], these last modes being polarized at a large angle $\sim 80°$ of the [20$\bar{1}$] direction. It is also remarkable that contrary to the ⟨110⟩ bisector, no anomaly of this kind is observed along ⟨011⟩, where at least one acoustic mode should have a polarization component along **a**.

The more conspicuous feature of this anomaly is the frequency dispersion that reaches an unusual magnitude in *A*-TCNB. Figure 5(a) shows the effect of this dispersion on the velocity of the QL mode propagation along **a**. This mode was observed with two different scattering geometries: backscattering and a small-angle geometry, where the scattering angle inside the crystal is defined by the refractive index $\theta_i = 2\sin^{-1}(n\sqrt{2})^{-1}$, which here equals 46°. Such a value in Eq. (1) yields a small Brillouin shift of about 8 GHz, whereas in backscattering ν_B reaches 22 GHz. Most of the dispersion takes place in the low-temperature phase, and the magnitude of the anomaly is larger at lower frequencies. This dispersion is still more visible in the Brillouin linewidth evolution, since, for different Brillouin shifts, the linewidth peaks at temperatures that are noticeably different. Figure 6 shows the linewidth versus temperature for different modes and scattering geometries.

This dispersion is the proof of the coupling of sound waves with another mode, and, consequently, the shape of the Brillouin lines is modified by this coupling. They may even become no longer Lorentzian for large couplings. Figure 7 displays two Brillouin spectra recorded at 207 K in a right-angle scattering geometry showing phonons propagating along ⟨101⟩ and ⟨10$\bar{1}$⟩. The anisotropy of the anomaly is obvious with a broad QL mode along ⟨10$\bar{1}$⟩, whereas along ⟨101⟩ the QL mode is not broadened at all. In fact, along ⟨101⟩ the anomaly is very large $[\Delta V^2/V^2(T_c)] = 45°$ for the QT mode and the related Brillouin profile is more complex than a simple Lorientzian, and this is also probably true for the QL mode along ⟨10$\bar{1}$⟩. These lines are asymmetric with an important shoulder on the low-frequency side of the Brillouin line, and, at 207 K, these lines are close to their maximum linewidth. A similar line shape is also observed for the QL mode propagating along **a**.

The understanding of the origin of these anomalies is a major point of interest. In Table III we recall the unit vectors defining the propagation vector **q** and the polarization **u**, computed with the room-temperature C_{ij} values of some measured acoustic phonons. The following columns give the absolute, $\Delta V^2 = V^2(T_c) - V^2_{\min}$, and relative, $\Delta V^2/V^2(T_c)$, elastic anomalies, whereas the last column shows $(\mathbf{u}\cdot\mathbf{L})^2$, where **L** is the unit vector pointing along the molecular long axis. This scalar product varies roughly as $\Delta V^2/V^2(T_c)$ in the case of the largest

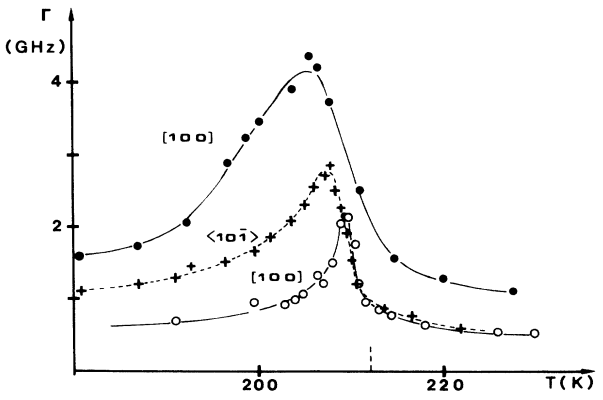

FIG. 6. Measured Brillouin linewidth of the QL mode propagating along **a** measured in a backscattering (●) and small-angle geometry (○) and of the QL mode propagating along ⟨10$\bar{1}$⟩ measured at right-angle scattering (+) (lines are guides for the eye).

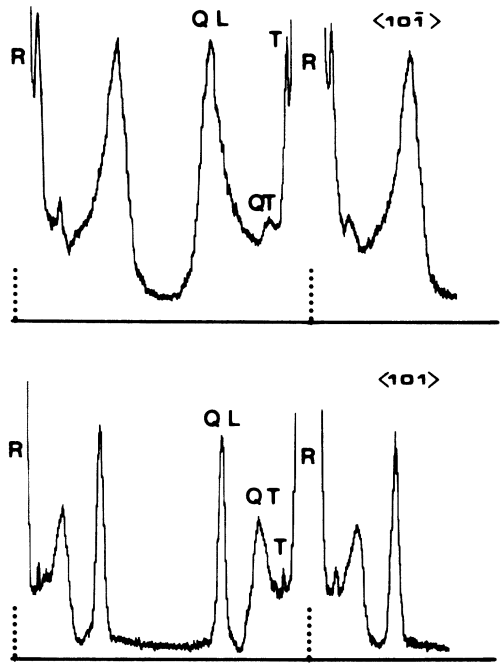

FIG. 7. Brillouin-scattering spectra recorded at 207 K in a right-angle geometry along the ⟨10$\bar{1}$⟩ (above) and ⟨101⟩ (below) directions in the (*V*,*V*) polarization. QL and QT indicate, respectively, quasilongitudinal and quasitransverse modes, whereas *T* corresponds to the true transverse mode polarized along **b**, which is detected here due to some polarization leakage. The free spectral range indicated by the dotted line at the location of the Rayleigh line (*R*) is 39.15 GHz.

TABLE III. Magnitude of the anomalies of $\Delta V^2 = V^2(T_c) - V^2_{\min}$ for some acoustic phonons characterized by their propagation vector **q** with polarization at 293 K: **u** (293 K), the absolute ΔV^2, and relative magnitudes $\Delta V^2/V^2(T_c)$ of the anomalies are compared to $(\mathbf{u},\mathbf{L})^2$. The last column gives the variation of C'_{11} which would produce the corresponding ΔV^2.

q	**u** (293 K)	ΔV^2 (km^2/s^{-2})	$\frac{\Delta V^2}{V^2(T_c)}$ (%)	$(\mathbf{u}\cdot\mathbf{L})^2$	$\Delta C'_{11}$ (GPa)
$\begin{bmatrix}1\\0\\0\end{bmatrix}$	QL $\begin{bmatrix}0.938\\0\\-0.240\end{bmatrix}$	4.21 (20 GHz) 4.82 (8 GHz)	29 34	0.93	6.6 7.6
$\begin{bmatrix}1/\sqrt{2}\\0\\-1/\sqrt{2}\end{bmatrix}$	QL $\begin{bmatrix}0.910\\0\\-0.414\end{bmatrix}$	3.76	25.5	1	6.3
$\begin{bmatrix}1/\sqrt{2}\\1/\sqrt{2}\\0\end{bmatrix}$	QL $\begin{bmatrix}0.842\\0.508\\0.181\end{bmatrix}$	2.11	20	0.50	9.1
$\begin{bmatrix}1/\sqrt{2}\\0\\1/\sqrt{2}\end{bmatrix}$	QT $\begin{bmatrix}0.725\\0\\-0.688\end{bmatrix}$	2.10	45	0.90	9.6
$\begin{bmatrix}0\\0\\1\end{bmatrix}$	QT $\begin{bmatrix}0.982\\0\\-0.190\end{bmatrix}$	1	20.5	0.97	7.9
$\begin{bmatrix}1/\sqrt{2}\\0\\-1\sqrt{2}\end{bmatrix}$	QT $\begin{bmatrix}0.413\\0\\0.914\end{bmatrix}$	0.2	6.7	0.002	6.3
$\begin{bmatrix}1/\sqrt{2}\\0\\1/\sqrt{2}\end{bmatrix}$	QT $\begin{bmatrix}0.688\\0\\0.725\end{bmatrix}$	0.1	0.01	0.33	~ 1
$\begin{bmatrix}0\\0\\1\end{bmatrix}$	QT $\begin{bmatrix}0.190\\0\\0.982\end{bmatrix}$	0.09	0.01	-0.23	~ 1
$\begin{bmatrix}1/\sqrt{2}\\1/\sqrt{2}\\0\end{bmatrix}$	QT $\begin{bmatrix}0.476\\-0.858\\0.191\end{bmatrix}$	$\epsilon \sim 0$	~ 0	0.13	11.3ϵ
$\begin{bmatrix}0\\1/\sqrt{2}\\1/\sqrt{2}\end{bmatrix}$	QT $\begin{bmatrix}0.960\\-0.105\\-0.258\end{bmatrix}$	$\epsilon' \sim 0$	~ 0	0.99	$30\epsilon'$

anomalies except for the QT mode propagating along **c*** and polarized in the (**a**,**c**) plane. Moreover, if this quantity is relevant in the case of large anomalies, it completely loses any significance for nonanomalous phonons such as along $\langle 011 \rangle$ or [010]. The last column of this table, related to $\Delta C'_{11}$ is dealt with in the following section. Nevertheless, this table underlines the importance of the phonons polarized along the molecular long axis for the interaction with ordering quantities. It is also consistent with the model of the rotation of the *A* molecules in their planes because any molecular translation along this long axis strongly modifies the environment and the rotation possibilities of these molecules.

DISCUSSION AND THEORY

This SPT is a nonferroic transition driven by a small irreducible one-dimensional representation. The active representation of the *Z* point[21] $(0, \pi/a, 0)$ or $(\pi/a, 0, 0)$, which is also called *M* by other authors,[12,13] is of the Bg symmetry and allows the following free-energy expansion:

$$F - F_0 = \frac{A_0}{2}(T - T_c)\eta^2 + \frac{B}{4}\eta^4 + \frac{D}{6}\eta^6 + \cdots + \tfrac{1}{2}\sum_{i,j=1,\ldots,6} C_{ij}\epsilon_i\epsilon_j + \tfrac{1}{2}\sum_{i=1,2,3,5} h_i\eta^2\epsilon_i + \tfrac{1}{4}\sum_{j=1,\ldots,6} g_j\eta^2\epsilon_j^2 + \cdots , \quad (8)$$

where ϵ_i denotes the components of the strain tensor, and η is the one-dimensional order parameter. The two last terms of the series describe the lowest-order couplings between strains and order parameter allowed by symmetry. The effects of these couplings on the elastic constants

have already been discussed in detail by many authors[22] and will only be recalled here.

The first term in h_i gives a static negative jump at T_c for the related elastic constant with a rounding of this step due to the effect of fluctuations. When the order-parameter fluctuations can follow the acoustic phonons, then this rounding looks like a relaxation effect. The magnitude of the anomally depends on the value of the h_i parameters that can be very different, obviously, h_3 is small and $h_2=0$, since there is no such anomaly for longitudinal modes along **b**. The largest remaining terms are then h_1 and h_5, which can produce anomalies on elastic constants such as C_{11}, C_{15}, C_{55} but the fifth column of Table III suggests a strongest interaction along the molecular long axis **L**. Consequently the simplest model would consist in a unique elastic anomaly for compressive waves along **L**, which we will call $\Delta C'_{11}$, with the prime symbol related to the elastic constants in the frame built with the **L** and **b** axis. The transformation of this tensor component by a rotation of an angle θ_L around the **b** axis induces the following variation on the other constants calculated in the (**a**,**b**,**c***) frame:

$$\begin{aligned}
&\Delta C_{11}=\Delta C'_{11}\cos^4\theta_L=0.739\Delta C'_{11}\ ,\\
&\Delta C_{33}=\Delta C'_{11}\sin^4\theta_L=0.020\Delta C'_{11}\ ,\\
&\Delta C_{55}=\Delta C_{13}=\Delta C'_{11}\cos^2\theta_L\sin^2\theta_L=0.1206\Delta C'_{11}\ ,\\
&\Delta C_{15}=-\Delta C'_{11}\cos^3\theta_L\sin\theta_L=-0.299\Delta C'_{11}\ ,\\
&\Delta C_{35}=-\Delta C'_{11}\sin^3\theta_L\cos\theta_L=-0.049\Delta C'_{11}\ ,
\end{aligned} \tag{9}$$

where $\theta_L=-(\mathbf{a},\mathbf{L})\simeq+22°$. Then according to Eq. (9), $h_1\approx 6h_3\approx -2.5h_5$.

With these relations and the elastic constants computed at room temperature it is possible to compute the effect of these anomalies on some sensitive acoustic modes and then $\Delta C'_{11}$ can be determined. A reasonable value of $\Delta C'_{11}$ averaged over the modes, which undergo a noticeable anomaly and are listed in the last column of Table III, is given by $\Delta C'_{11}=7.6\pm1.5$ GPa. Moreover this description predicts very small anomalies along ⟨011⟩ and for the modes along other directions where such anomalies have not been observed.

The other possible cause of a negative jump could be an anomaly concerning C'_{55}, but it contradicts our experimental observations, which underline the privileged directions of the long molecular axis for the polarization of waves, and then, if such an anomaly could exist, it would produce elastic constants variations satisfying the following relations:

$$\Delta C_{11}=\Delta C_{33}=-\Delta C_{13}\ . \tag{10}$$

These equalities are obviously not verified by experiments, and, since ΔC_{33} is practically zero, it implies that the contribution of $\Delta C'_{55}$ to ΔC_{11} is also negligible. This means that $\Delta C'_{55}$ is indeed very small and can be ignored.

Nevertheless it is difficult to derive an accurate value of $\Delta C'_{11}$ due to the dispersion that decreases the magnitude of the measured anomalies when frequency increases, but, on the other hand, this effect can be used in order to determine the dynamical response of the order parameter.

If one assumes a Landau-Khalatnikov mechanism for the attenuation of the sound waves in the low-temperature phase, we can describe the dispersion of the elastic constants by a relaxation mechanism governed by a single relaxation time τ, which, in the case of a mean-field approximation, diverges like $(T_c-T)^{-1}$. The expression that relates the Brillouin shifts and the related linewidth to the relaxation time are well known:[22]

$$\begin{aligned}
&\nu^2=\nu_\infty^2-\frac{1}{4\pi^2}\frac{A^2}{1+4\pi^2\nu^2\tau^2}\ ,\\
&\gamma=\gamma_\infty+\frac{1}{2\pi}\frac{A^2\tau}{1+4\pi^2\nu^2\tau^2}\ ,
\end{aligned} \tag{11}$$

where ν_∞ and γ_∞ are the Brillouin shift and linewidth in the absence of relaxation, i.e., at very large values of τ, A being a coupling parameter taken as a constant. Since, in the single relaxation-time approximation, γ is maximum at a temperature T_m defined by $2\pi\nu(T_m)\tau(T_m)=1$, we can obtain a determination of $\tau(T_m)$ for all the temperatures where a maximum of linewidth is observed for any acoustic mode displaying this kind of anomaly, since we are sure that all these anomalies have the same origin, i.e., $\Delta C'_{11}$. Another determination can be obtained by plotting $(\gamma_{(T)}-\gamma_\infty)/(\nu_\infty^2-\nu_{(T)}^2)$ which equals $2\pi\tau(T)$. This is a reliable determination of $\tau(T)$ if the true phonon linewidth γ and the frequency ν_∞ can be found. It also assumes that the Brillouin line shape can be reasonably described by a Lorentzian. The linewidth can be obtained by a deconvolution of the recorded profile from the instrumental function. The correct determination of ν_∞ is more tedious, since critical fluctuations also decrease the Brillouin frequency in the vicinity of T_c with a singular contribution at this temperature. This effect is different from the Landau-Khalatnikov damping, since it involves fluctuations in the whole Brillouin zone, provided that they are related by opposite wave vectors. This difference allows the observation of the fluctuation effect even in the high-temperature phase where the critical fluctuations do not occur in the Brillouin-zone center. Moreover the coupling constants with acoustic waves have been shown to be the same as for the Landau-Khalatnikov mechanism.[23]

Another trouble arises at lower temperatures, since, as already shown,[22] a contribution proportional to η^2 decreases the apparent magnitude of the relaxation of the elastic constant as soon as the temperature goes below T_c. It results from the mixing of these effects that Eq. (11), which represent a first-order approximation, are only valid in a limited temperature range below T_c. Figure 8 shows the evolution of the inverse of the relaxation time with data obtained from the maxima of the Brillouin linewidths and from the combination of Eqs. (11). In this figure we can observe some data scattering, particularly for those obtained from small-angle scattering along [100]. In fact, for small-angle scattering as well as for backscattering, we have determined the phonon linewidth not from a true deconvolution but from the abacus built

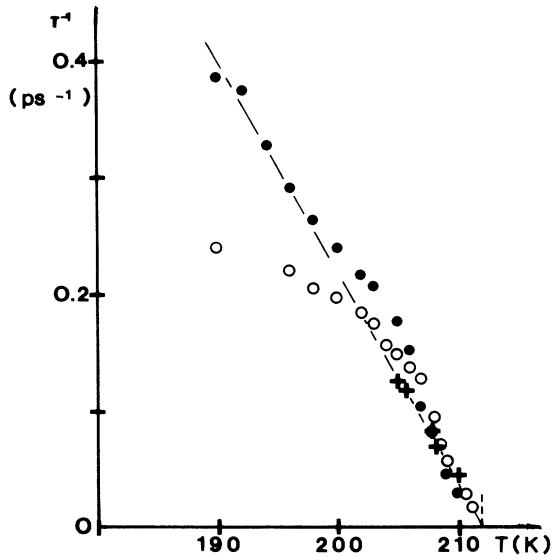

FIG. 8. Evolution of τ^{-1} vs temperature in the low-temperature phase determined from Eq. (10) applied to data recorded with the QL mode propagating along **a** in backscattering (●), small-angle geometries (○) and also from the maximum linewidth of other modes (+).

by Lindsay and Shepherd,[24] and, in the small-angle geometry, collecting optics may add a significant contribution to the measured linewidth, and this effect was probably not sufficiently taken into account. However, the agreement between the different determinations of τ^{-1} is reasonable when the measured linewidths are large. In a first approximation this quantity varies linearly near T_c so that we can assume mean-field behavior for the relaxation time with a value of T_c very close to 212 K:

$$\tau(T)\simeq\frac{5\times10^{-11}}{212-T}=\frac{\tau_0}{T_c-T}\ . \tag{12}$$

A better analysis would require to take into account the effect of the critical fluctuations as underlined by Yao *et al.*[23]; such an analysis is now being elaborated, but it requires many independently measured parameters.

The last term in the Landau free energy [Eq. (8)] couples the square of each strain with the square of the order parameter. This coupling gives an increase of the elastic constant below T_c in proportion with the square of the order parameter. When this increase is small, the related sound-velocity variation ΔV_i can, in a first-order approximation, be described by the same variation:

$$\Delta C_{ii}=g_i\eta^2\simeq2\rho V_1\Delta V_1\ . \tag{13}$$

This kind of coupling is more visible for the modes that do not present the negative jump discussed above. In particular, it is the case of the true transverse (T) modes related to the B_g-type strains ϵ_4 and ϵ_6. The largest effects are, once again, encountered for modes propagating along **a** and the second bisector $\langle 10\bar{1}\rangle$. It is also visible in Fig. 5(c) that the T velocities along $\langle 10\bar{1}\rangle$ continuously increase below T_c. It reaches the T velocity along $\langle 101\rangle$ at 180 K and becomes even larger below. Since these velocities are related by

$$\rho V_i^{T_2}=X^{T}_{\substack{\langle 101\rangle\\\langle 101\rangle}}=\frac{C_{44}+C_{66}}{2}\pm C_{46}\ , \tag{14}$$

it follows that C_{46} decreases in the low-temperature phase.

Here also it seems reasonable to express these elastic constants in the frame defined by **L** and **b**. If we then assume only one coupling constant, g'_6, which is suggested by the magnitude of the T anomalies along **a** and $\langle 101\rangle$, we can express the deviations from the high-temperature phase with only one deviation $\Delta C'_{66}$ and the same θ_L angle in the (**a**,**b**,**c***) frame:

TABLE IV. Magnitude of the sound-velocity variations induced by a biquadratic coupling $Q^2(\epsilon')^2_6$: $\mathbf{q}_i$ is the propagation unit vector, $\mathbf{u}_i$ the polarization unit vector, and V_1^2 the square of the velocity of this mode. In the fourth column $\Delta X_i=\rho\Delta V_i^2$ is normalized to the variation of $\Delta C'_{66}$, which is the elastic constant variation: $\Delta C'_{66}=g'_6\eta^2(T)$ computed at 192 K from anomalies on T modes.

$\mathbf{q}_i$	$\mathbf{u}_i$ (293 K)	V_i^2 (192 K)-V_i^2 (212 K) (km^2/s^2)	$\frac{\Delta X_i}{\Delta C'_{66}}$	$\Delta C'_{66}$ (192 K) (GPa)
$\begin{bmatrix}1/\sqrt{2}\\0\\-1/\sqrt{2}\end{bmatrix}$	$T\ \begin{bmatrix}0\\1\\0\end{bmatrix}$	0.29	0.85	0.45
$\begin{bmatrix}1/\sqrt{2}\\0\\1/\sqrt{2}\end{bmatrix}$	$T\ \begin{bmatrix}0\\1\\0\end{bmatrix}$	0.046	0.15	0.41
$\begin{bmatrix}1\\0\\0\end{bmatrix}$	$T\ \begin{bmatrix}0\\1\\0\end{bmatrix}$	0.29	0.85	0.45
$\begin{bmatrix}0\\1\\0\end{bmatrix}$	$T\ \begin{bmatrix}1\\0\\0\end{bmatrix}$	0.17	0.6	0.37

$$\Delta C_{44}=\Delta C'_{66}\sin^2\theta_L=0.140\Delta C'_{66}\ ,$$
$$\Delta C_{66}=\Delta C'_{66}\cos^2\theta_L=0.86\Delta C'_{66}\ , \quad (15)$$
$$\Delta C_{46}=-\Delta C'_{66}\cos\theta_L\sin\theta_L=-0.347\Delta C'_{66}\ ,$$

where $\Delta C'_{66}(T)=g'_6\eta^2(T)$. Then we know that $g_6\simeq -2.5g_4$, but we cannot determine which one is negative.

The effect of these variations on $X=\rho V^2$ can easily be computed for the measured modes, and it is shown in the fourth column of Table IV in the $\Delta C'_{66}$ unit. The other columns describe the mode propagation, polarization, the difference between values of V_1^2 at T_c and T_c-20 K, and the variation of C'_{66} at T_c-20 K, which would give the recorded variation of X. The agreement among all these values of $\Delta C'_{66}$ is remarkable, since the average value is $\Delta C'_{66}=0.42\pm0.05$ GPa with a relative error of only about 10%.

The remarkable result of this analysis concerns C_{44}, which still was not observed at these temperatures, but the above analysis reveals that it should not increase by more than 0.06 GPa. This value corresponds to an increase of only 40 m/s for the velocity of the T mode propagating along **c***, so that there is no significant modification for this mode in the low-temperature phase.

CONCLUSION

This Brillouin-scattering study points out several important features relating to the crystalline structure with respect to the elastic properties and the elastic anomalies that take place at the transition temperature. The main points directly related to the structure are, on the one hand, the maximum of velocity, which occurs along the molecular axis as usual for Van der Waals–type crystals and, on the other hand, the quasisoft shearing of the stack architecture within the (102) planes. Unstable acoustic modes related to this structure were predicted by an earlier lattice-dynamics computation,[13] but contrary to this prediction we have shown, even without a direct recording of one of these modes, that one mode is very slow, though it does not exhibit any unstable behavior. However, this very small velocity (<500 m/s) reveals a very small interaction between molecular (102) layers indicating a very weak charge-transfer interaction.

This study is also a proof that the reorientation of anthracene molecules indeed drives this SPT, since the elastic anomalies recorded by Brillouin scattering can all be reliably interpreted as the result of modifications of the elastic behavior along the anthracene molecular long axis. However, this study makes no conclusions about the regime of this transition, because the negative jump anomaly exhibited by C'_{11} can equally well be driven by a relaxation mechanism or a soft mode. What Brillouin scattering can probe is a dispersion in the GHz region, indeed this dispersion is unusually large for A-TCNB, and the relaxation time obtained here is larger than for a true soft-mode like, for example, $\tau_0\sim5$ ps K in chloranil.[25] The value we have obtained here, $\tau_0\sim50$ ps K, is much closer to the so-called intermediate regimes as in the TGS family ($\tau_0\sim30$ ps K) than to true order-disorder SPT, as in $NaNO_2$ ($\tau_0\sim16$ ns K).[26] The recorded Brillouin spectra have also some similarities with those obtained by Kruger *et al.*[27] with squaric acid, which undergoes an order-disorder antiferroelectric SPT with a relatively fast dynamics.

This study also proves that the SPT of A-TCNB is a continuous phase transition. The critical temperature has been unambiguously determined on the same crystal by two kinds of elastic anomalies, which give the same numerical value $T_c=212\pm0.5$ K, but later experiments performed on crystals grown from pure chemicals of different origin undergo the same phase transition with the same elastic anomalies at $T'_c\simeq215$ K. We then think that this temperature reveals a very large sensitivity of the SPT to impurities as is confirmed by the temperature shift observed in mixed A-phenanthracene–TCNB crystals.[28] T_c can actually be sensitive to the presence of defects, since it is also very strongly pressure dependent, ~32 K/kbar.[16] We think that the scattering of the T_c values in the literature could be related to defects or impurities.

We now need a more advanced analysis, which should integrate thermodynamical data, elastic, and soft-mode behavior as observed through the coupling with acoustic waves and compared to direct Raman and neutron-scattering observations[29] in order to obtain a better understanding of the dynamics this transition.

ACKNOWLEDGMENTS

We are grateful to Professor T. Luty for fruitful discussions and communication of his work prior to publication and to Dr. L Toupet for his material help for drawings. Groupe de Physique Cristalline is Unité de Recherche Associeé No. 040804 du Centre National de la Recherche Scientifique.

[1]A. Ponte Goncalves, Chem. Phys. **19**, 397 (1977).
[2]W. Auch, W. Steudle, J. U. Von Schütz, and H. C. Wolf, Phys. Status Solidi A **49**, 563 (1978).
[3]H. Möhwald, E. Erdle, and A. Thaer, Chem. Phys. **27**, 79 (1978).
[4]J. M. Park and A. H. Reddoch, J. Chem. Phys. **74**, 1519 (1981).
[5]L. Pasimeni and C. Corvaja, Solid State Commun. **53**, 213 (1985).
[6]H. Möhwald and A. Thaer, Phys. Status Solidi A **50**, 131 (1978).
[7]A. Mierzejewski, C. Ecolivet, G. S. Pawley, T. Luty, A. Girard, and M. H. Lemée, Solid State Commun. **65**, 431 (1988).
[8]H. Tsuchiya, F. Marumo, and Y. Saito, Acta Crystallogr. B **28**, 1935 (1972).
[9]J. Stezowski, J. Phys. Chem. **83**, 550 (1979).
[10]J. C. A. Boeyens and D. C. Levendis, J. Chem. Phys. **80**, 2681

(1984).
[11]J. Lefebvre, G. Odou, M. Muller, and A. Mierzejewski, Mater. Sci. **14**, 45 (1988); Acta Crystallogr. B **45**, 323 (1989).
[12]T. Luty and B. Kuchta, J. Chem. Phys. **85**, 4032 (1986).
[13]K. H. Brose, T. Luty, and C. J. Eckhardt, Chem. Phys. Lett. **137**, 17 (1987).
[14]T. Luty and J. Lefebvre, J. Chem. Phys. **90**, 7346 (1989).
[15]W. C. Kerr and A. R. Bishop, Phys. Rev. B **34**, 6295 (1986).
[16]C. Ecolivet, M. H. Lemée, and M. Bertault, Mater. Sci. **14**, 55 (1988); M. Boumaza, Ph.D. thesis, University of Rennes, 1988 (unpublished).
[17]C. Ecolivet, M. Sanquer, J. Dewitte, and R. Pellegrin, J. Chem. Phys. **78**, 6317 (1983).
[18]A. Wynchell, *The Optical Properties of Organic Compounds* (Academic, New York, 1954).
[19]C. Ecolivet, J. Phys. (Paris) Colloq. **42**, C6-578 (1981).
[20]H. B. Huntington, S. G. Gangoli, and J. L. Mills, J. Chem. Phys. **50**, 3844 (1969).
[21]J. Zak, A. Cahser, H. Gluck, and Y. Gur, *The Irreducible Representations of Space Groups* (Benjamin, New-York, 1969).
[22]J. P. Benoit, F. Thomas, and J. Berger, J. Phys. (Paris) **44**, 841 (1983).
[23]W. Yao, H. Z. Cummins, and R. H. Bruce, Phys. Rev. B **24**, 424 (1981); A. Yoshihara, E. R. Bernstein, and J. C. Raich, J. Chem. Phys. **79**, 445 (1983).
[24]S. M. Lindsay, S. Burgess, and I. W. Shepherd, Appl. Opt. **16**, 1404 (1977).
[25]A. Girard, Y. Delugeard, and C. Ecolivet, J. Phys. C **4**, 601 (1987).
[26]H. Z. Cummins, in *Light Scattering near Phase Transitions,* edited by H. Z. Cummins and A. P. Levanyuk (North-Holland, Amsterdam, 1983).
[27]J. K. Kruger, H. D. Maier, J. Petersson, and H. G. Unruh, Ferroelectrics **25**, 621 (1980).
[28]E. Erdle and M. Möhwald, Z. Naturforsch. Teil A **35**, 236 (1970); J. Lefebvre and A. Mierzejewski (private communication).
[29]Ph. Bourges, C. Ecolivet, A. Mierzejewski, Y. Delugeard, and A. Girard, in *Phonons 89,* edited by S. Hunklinger, W. Ludwig, and G. Weiss (World Scientific, Singapore, 1990) p. 1147.

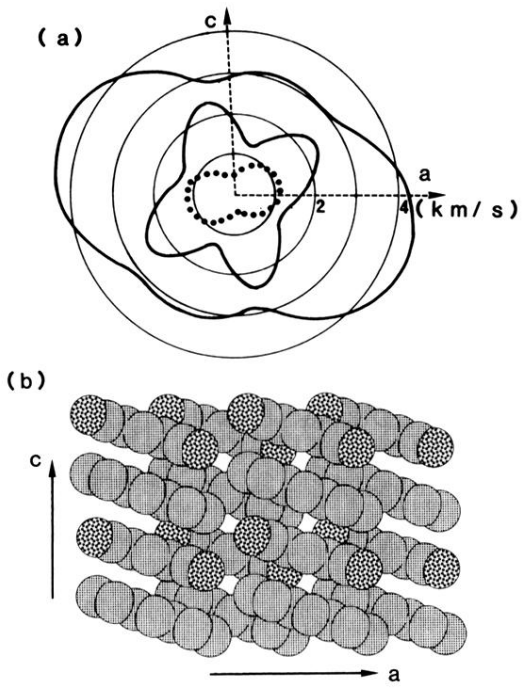

FIG. 1. Sound-velocity diagram (a) and projection of the molecular packing in the (**a**,**c**) plane (b). The dotted line corresponds to the true transverse mode polarized along **b**, whereas the two other lines are QT and QL modes. In the molecular projection, anthracene molecules are represented without hydrogen atoms. Carbon atoms are uniformally shaded, whereas nitrogen atoms are dotted.

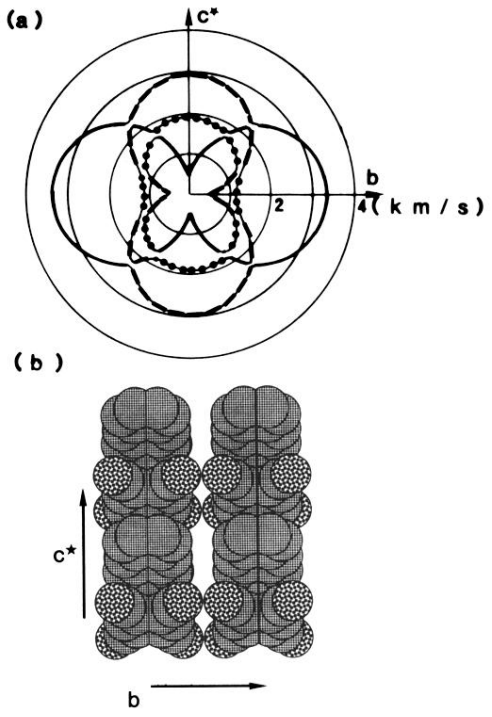

FIG. 2. Sound velocity (a) and projection of the molecular packing in the ($\mathbf{b},\mathbf{c}^*$) plane (b). The three velocities never cross but dots are related to a QT mode mostly polarized along **a**, whereas dashes indicate a polarization along $\mathbf{c}^*$ and the bold line indicates a polarization along **b**.